Effect of process parameters on thermal and mechanical properties of polymer-based composites using fused filament fabrication

Khaled Benfriha[1] | **Mohammad Ahmadifar**[1,2] | **Mohammadali Shirinbayan**[2] | **Abbas Tcharkhtchi**[2]

[1]Arts et Metiers Institute of Technology, CNAM, LCPI, HESAM University, Paris, France

[2]Arts et Metiers Institute of Technology, CNAM, PIMM, HESAM University, Paris, France

Correspondence
Mohammad Ahmadifar and Mohammadali Shirinbayan, Arts et Metiers Institute of Technology, CNAM, PIMM, HESAM University, F-75013 Paris, France.
Email: mohammad.ahmadifar@ensam.eu and mohammadali.shirinbayan@ensam.eu

Abstract

The fused filament fabrication (FFF) process of polymer-based composites has been developed due to its capability to make complex geometries and shapes with reasonable mechanical properties. However, the improvement of mechanical properties of the obtained parts and products are still under study and are interesting for designers. There are several strategies to enhance these desired properties of produced pieces, for example optimizing the process parameters and/or using different architecting designs. This paper presents the effect of some overriding process parameters (liquefier temperature, print speed, layer height, and platform temperature) on the temperature evolution and mechanical behavior of PA6 reinforced with chopped carbon fibers produced by FFF. Due to deposition of multilayers, there is a cyclic profile of temperature in the FFF process, which is a considerable note related to fabrication and consequently the strength of the manufactured parts. In parallel with the study of process parameters effect, this cyclic temperature profile has been measured. The preliminary results related to physicochemical and mechanical properties revealed that differences in crystallinity percentage exist and failure stress/strain can be considered as an indicator to evaluate the mechanical properties of FFF manufactured products. Moreover, measuring the temperature profile of the deposited filaments revealed that process parameters have a considerable influence on the cooling process of deposited filaments which itself affects the bonding of adjacent filaments. The higher temperatures led to slower cooling rate. Finally, the results confirm the impact of mentioned parameters roles on the bonding formation in the FFF process and also the subsequent obtained mechanical properties of the printed parts. Therefore, selection of the optimized and suitable process parameters is an important design consideration.

KEYWORDS

composite, FFF, mechanical properties, process parameters, temperature

1 | INTRODUCTION

Additive manufacturing (AM) is the manufacturing method for fabricating objects from the three-dimensional (3D) computed-aid design (CAD) model, and it is a layer-by-layer manufacturing process. While the subtractive manufacturing process is introduced as another category of the 3D printing methods, which is based on successively removing material away from a solid block of material to obtain the desired 3D object. AM also known as free-form fabrication, layer manufacturing, additive processes, additive techniques, and solid free-form fabrication.[1] AM method begins with CAD software and designing to prepare the desired model. Then it will be sliced into a predefined number of layers and fabricated sequentially. Moreover, AM is utilized widely because of its capability to manufacture objects with complex shapes, which are hard to be fabricated by means of conventional methods.[2,3] Compared to conventional methods, AM process reduces post processing and material wastes. Also it has appealed the attentions because of its economical features for rapid prototyping and production applications.[4] Different materials can be used as raw material of AM and be printed such as metals, ceramics, polymers, biomaterial, and organic compounds.[5,6] In the past decades, AM has been involved in wider various applications. The most important applications of AM Include the aerospace, automotive, architectural design, and medical industries.[7–9]

AM techniques after several decades such as stereolithography, fused filament fabrication (FFF) or fused deposition modeling, selective laser sintering (SLS), selective laser melting, multi-jet modeling, laminated object manufacturing, and SL, have been developed.[10–15] Among the stated methods, the FFF process due to less material wastage, less expensive used materials and tools is more cost-effective than the other processes. Therefore, FFF is currently the most widely available AM platform.[7]

The most widely used AM methods for processing polymer composites are FFF and SLS, while the FFF method has been considered as the more beneficial process. Some advantages of FFF process in comparison with other AM methods are ability to deposit several materials simultaneously, low input energy, material availability, and minimum waste of material because they are less prone to degradation, less expensive machines and materials, no need for subsequent chemical processing and machining, and availability wide range of printers at different prices.[16–25]

The FFF printer consists of several parts. As for the brief of the FFF process, the filament is fed into an extrusion head, first. The extrusion head is controlled by temperature and heated to a semiliquid state. Then, the used raw material transformation from solid-state in the filament form to the molten state occurs in a liquefier area. The solid portion of the raw material, which remains unmelted, acts as a piston to push the melt through a nozzle. The process of FFF in three axes (X, Y, and Z) of extrusion-like process is done in the form of a thin ribbon and confirms the bonding of extruded and printed filaments in each layer.[20,26] In FFF, the desired specimens and structures can be fabricated from CAD.[24] On the other hand, the FFF method has limitations, such as limited mechanical properties of the manufactured parts and specimens and limited range of available raw materials for selection. In fact, thermoplastic materials mostly are used as FFF raw materials.

The majority of the materials currently used for FFF are the amorphous material or thermoplastic with low levels of crystallinity such as Acrylonitrile butadiene styrene (ABS) and PLA, which cause less shrinkage in the fabricated parts. Also fiber reinforced polymers can be used in the FFF process and expand its application in aerospace and automobile industries due to its economical feature and reasonable mechanical properties, the FFF process is also used to manufacture the composite parts.[27,28]

A composite material composed of two or more constituent materials with different properties, which offers overall performance compared to the individual constituent members.[29] Due to the time and location of the fiber adding, there are three methods for the FFF process of polymer matrix composite. The first method is including (Figure 1A) when the used filament itself is a composite and contains fiber reinforcement. Second method is related to the situation that the filament and fiber reinforcement are unified when they pass through the liquefier and print nozzle (Figure 1B). The third method needs two independent extruders each one with an independent nozzle (Figure 1C).[30]

Abhinav and Irfan,[31] have studied the impact of the bed temperature, primary layer thickness, and infill pattern (rectilinear, honeycomb, and triangular) on the mechanical properties. First, samples were printed by "Atharva Mega 3 Make" 3D-printer and the used material was Polylactide (PLA). The samples were applied to flexural and tensile tests. According to the obtained results, it was found out that increase in bed temperature initially increased the tensile strength, and then decreased it. The obtained results among the three selected infill patterns, triangular, and honeycomb showed better tensile strength. Also increasing the primary layer thickness and increased tensile strength. Shilpesh and Rajpurohit[32] have studied the effects of raster angle, layer height, and raster width on tensile strength of FFF printed PLA parts. In this study, five different values of the layer height (100, 150, 200, 250, and 300 mm) and four different

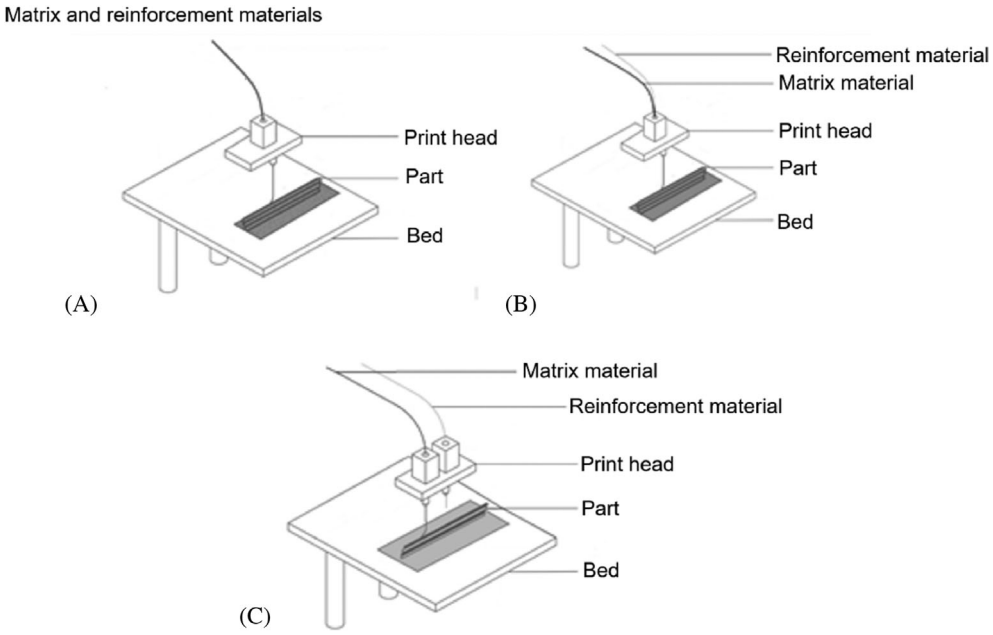

FIGURE 1 Fused filament fabrication reinforced with: (A) Composite filament (as raw material), (B) Combined filament and fiber through the print head, and (C) Combined filament and fiber with two independent nozzles[30]

values of the raster width (400, 500, 600, and 700 mm) were considered. It was stated that the tensile strength increased by increasing the raster width but decreased by voids presence. The raster angle had the maximum impact on the tensile strength of the printed parts. Precisely at the raster angle of 0°, the highest tensile strength was observed. Also as the layer height decreases, the tensile strength increases due to larger bonding area among layer interfaces. Ćwikła et al.,[33] investigated the impact of infill pattern, infill density, and shell thickness, on mechanical properties of FFF 3D-printed parts. The used material in the study was ABS and the used 3D printer machine was "Prusa i3 RepRap." The obtained results showed that, as shell thickness of the printed specimens increased and when there is an infill pattern other than honeycomb, the strength increases realized that for achieving a lightweight and durable element, shell thickness should be 2–3 layers and best infill pattern is honeycomb with fill density of about 40%–50%. Christiyan et al.,[34] studied the printed ABS composite (ABS + hydrous magnesium silicate composite) parts, by FFF process. And specimens with different layer thickness (0.2, 0.25, and 0.3 mm) and different printing speeds (30, 40, and 50 mm/s) considered and tensile and flexural tests applied to the specimens. According to the results, the most tensile and flexural strength obtained in layer thickness of 0.2 mm and printing speed of 30 mm/s. In other words, by selecting lower printing speed and lower layer thickness, the maximum tensile and flexural strength were obtained. Durga et al.,[35] have studied the effect of layer thickness and liquefier temperatures ($T_{liquefier}$) on tensile strength of reinforced PLA by carbon fiber (CF). Three different values of the layer thickness (0.1, 0.2, and 0.3 mm) and different values of $T_{liquefier}$ (205, 215, and 225 mm) were considered. As a result, the highest tensile strength was observed in the sample with the minimum layer thickness and highest $T_{liquefier}$. Young-hyu choi et al.,[36] studied the Influence of bed temperature on heat shrinkage shape error of ABS. In this study, the head nozzle temperature of 240°C and the head speed of 50 mm/s were considered. Also the printing process was performed under bed temperature values of 50, 70, 90, and 110 °C. It was observed that the sample with lower bed temperature has the highest deformed shape error. On the other hand, laminating adhesion became poor if the bed temperature is more than 120°C. Ramesh et al.[37] studied the influences of process parameters such as fill density, layer height, and print speed for nylon parts which processed by FFF. Three different values of print speed (60, 65, and 70 mm/s) and different values of fill density (50%, 75%, and 100%) were considered. It has been observed that when the fill density was selected as 100%, the ultimate tensile strength, flexural strength, and Shore D hardness is maximum. Also in the high print speed the defect of wrapping was observed. Also the low print speed values caused the heat-affected zones. So far, a lot of research has been done on the effect of process parameters on the mechanical properties of different polymers such as PLA, ABS, and so forth. Now during this study, the effect of changing different parameters has been investigated on the mechanical and thermal properties, and also physical and chemical characterization of polyamide 6 (CF-PA6) composite which includes CF, and the effect of changing different parameters has been investigated and the properties of materials for parameters optimization in FFF process of CF-PA6 composite has been considered.

2 | MATERIAL DESCRIPTION, 3D PRINTER DEVICE, AND CHARACTERIZATION METHODS

2.1 | Material and sample preparation

The selected material for this study was PA6 reinforced with chopped CF. This material known commercially as Onyx will be referenced as CF-PA6 for the purposes of this study. In fact, the used CF-PA6 is introduced as a composite filament, which is also possible to be used as a matrix material for fabricating the continuous composite parts with Markforged 3D printers. According to the obtained results from pyrolysis of the used CF-PA6 filament, the chopped carbons with the mass content of 6.5% were distributed in PA6 as the matrix with the mass content of 93.5%.

Figure 1 was used as the desired and designed sample geometry in terms of the study of the influence of FFF process parameters on thermal and mechanical behaviors. The specimens were printed under the prepared and selected process parameters, according to Table 1. The locations of the required samples to apply the different tests and characterizations have been determined in Figure 2. The time–temperature evolution monitoring was done through the printing process of the introduced specimen, too. The FlashForge Adventurer 3 was considered as the used printer through this study.

2.2 | Process parameters classification

There are miscellaneous process parameters provided by different 3D printer machines. The process parameters play an important role in terms of the adhesion between the printed layers and mechanical property of the manufactured parts by the AM process. The main prepared process parameters by FlashForge Adventurer 3 printer, which were excerpted for this research are tabulated in Table 1.

In other words, the effects of four main process parameters of $T_{liquefier}$, bed platform temperature (T_{bed}), print speed (V), and layer height on the manufactured specimens by FFF were studied. The printing conditions of specimens for evaluation purposes of the $T_{liquefier}$, print speed, layer height, and T_{bed} effects are sorted as conditions NO. 1, 2, 3, and 4 in Table 1, respectively.

2.3 | Materials and methods

2.3.1 | Microscopic observation

The ZEISS Optical microscope (OLYMPUS BH2) with 100 and 200 m magnifications was utilized for observation of the used raw material, which was reinforced PA6 by about 6.5 wt% chopped (CF-PA6). As for qualitative observation of the printed specimens at the different selected process parameters, the scanning electron microscope (HITACHI 4800 SEM–high resolutions [better than 1 nm]) was applied.

2.3.2 | Differential scanning calorimetric

By means of differential scanning calorimetry (DSC), the difference of temperature between the sample and reference through the heating of the sample was determined.

TABLE 1 The excerpted FFF process parameters

Condition no.	$T_{liquefier}$ (°C)	T_{bed} (°C)	V (mm/s)	Layer height (mm)
1	220			
	230	25 ± 0.5	15	0.1
	240			
2			13	
	240	25 ± 0.5	15	0.1
			17	
3				0.1
	240	25 ± 0.5	15	0.2
				0.3
4		25 ± 0.5	15	
	240	45 ± 1		0.1
		62 ± 1		
		79 ± 1		

Abbreviation: FFF, fused filament fabrication.

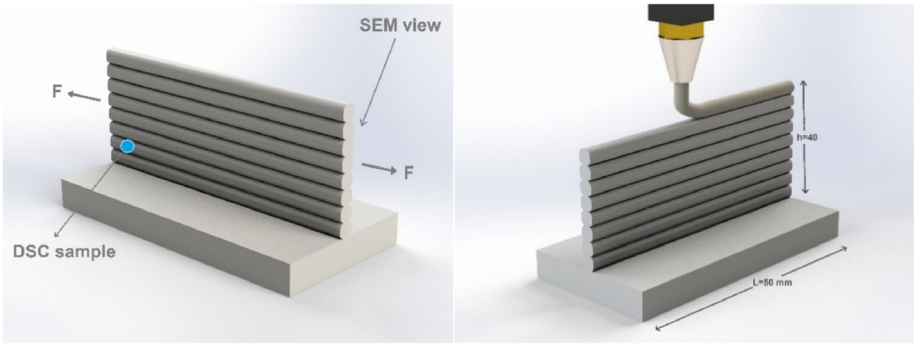

FIGURE 2 Schematic of the printed specimen

DSC provided the possibility to determine glass transition and crystallization temperature (T_c), also the heat capacity of the used CF-PA6 filament (as raw material) and the printed specimens at selected processing parameters. The measurements were carried out by means of DSC Q1000. The DSC characterization related to raw material (CF-PA6) was carried out in three ramps. The thermal history of the sample was erased in the first ramp. So the obtained results are measured under controlled conditions. The heating and cooling rate values were 10°C/min. While, the DSC characterization of the printed specimens were performed in two ramps (heating and cooling) with heating and cooling rate values were 10°C/min.

2.3.3 | DMTA measurement

Dynamic thermo-mechanical analysis (DMTA) flexural tests have been utilized to obtain the main glass transitions temperature of the printed sample made of reinforced PA6 with about 6.5 wt% chopped (CF-PA6). The stated measurement was carried out by DMA Q800 instrument from TA company. The flexural test was applied under the temperature range of 30–80°C, temperature rate of 2°C/min, the considered frequency of 1 Hz and applied force of 30 N.

2.3.4 | Quasi-static tensile test

The tensile specimen was cut from the printed specimen. The related dimension of used sample for mechanical test is according to ISO 527-2 (Figure 3). Quasi-static tensile experiments have been achieved with the INSTRON 4301 machine under the displacement rate of 5 mm/min. In fact, according to the printed specimen (Figure 2), the prepared mechanical test samples were from the printed single wall layers, which had 0° as raster angle. Minimum three specimens were prepared to perform tensile tests.

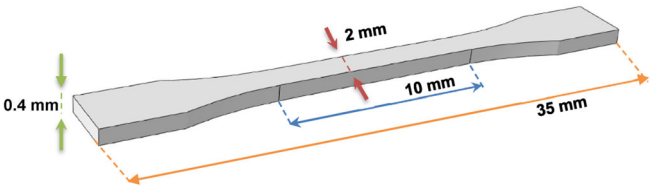

FIGURE 3 The geometry of the used specimen

2.4 | In situ evaluating of the temperature evolution of deposited filaments during FFF

Due to deposition of consecutive layers, there is a cyclic temperature profile in the FFF process. This is a significant phenomenon that affects the bonding of the deposited layers and the consequent strength of the printed object. So it is required to utilize equipment to be able monitor and measure the stated temperature evolution through the FFF process. For that, an Optris PI450 infrared camera was used by considering the determined distance from the extruder to achieve a suitable plain field of view of all consecutive printed and deposited layers (Figure 4). As for some technical data of the used infrared camera, the related frame rate, optical resolution, frequency, wavelength range, and accuracy values were 80 Hz, 382*288 pixels, 32 Hz, 8–14 μm, and 2%, respectively.

3 | RESULTS AND DISCUSSIONS

3.1 | Characterization of the used filament (raw material)

3.1.1 | Microstructure analysis

According to the observation of the CFs (observation) under the optical microscopy, the size range of the disturbed chopped CFs is about 10–312 μm (Figure 5A). Note that the diameter of used CF-PA6 filament was 1.75 mm. According to the optical observation of the

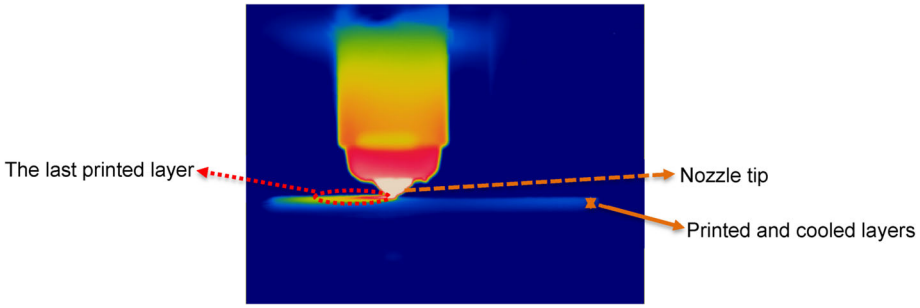

FIGURE 4 In situ monitoring of temperature profile through the deposition of consecutive layers in fused filament fabrication (FFF) process

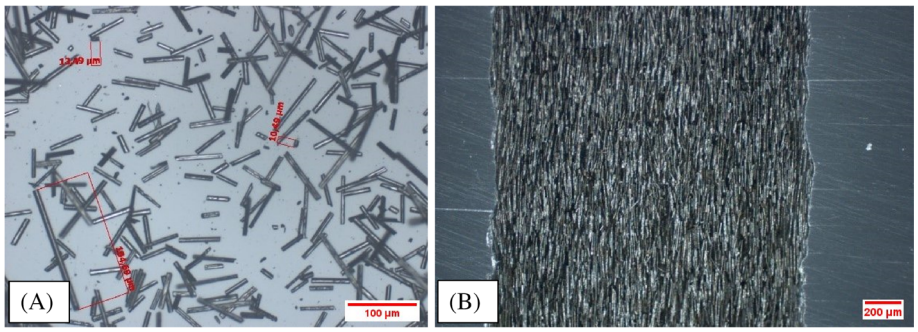

FIGURE 5 Microstructure observation: (A) After pyrolysis at 500°C for 5 h, and (B) Orientation of fiber in filament

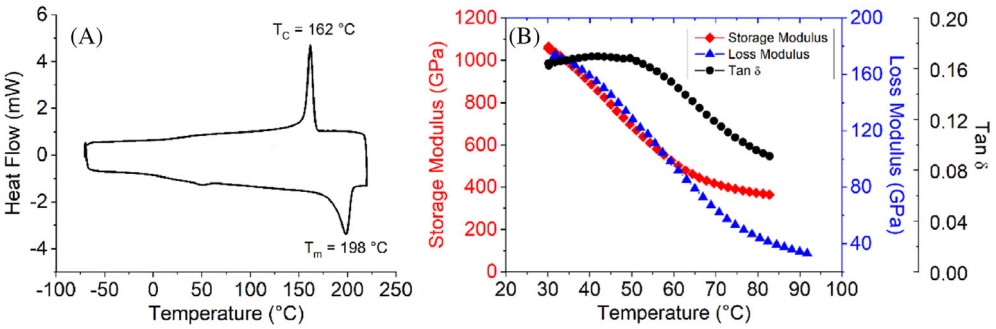

FIGURE 6 (A) Differential scanning calorimetry (DSC) and (B) DMA results for reference sample

CF-PA6 filament (Figure 5B), the chopped carbons of the CF-PA6 filament are oriented to the length of filament. The approximate unidirectional orientation of the short CF in length of CF-PA6 filament was due to the filament production process, which is the extrusion process.

3.1.2 | Thermal analysis

Figure 6 shows the results of the DSC and DMTA tests of CF-PA6. The glass transition temperature (T_g), the T_c, and the melting temperature (T_m) of this test respectively are reported in Table 2. According to the prerequisite for FFF in which the range between crystallization and T_m act as a semicrystalline material and due to the phase transformation, diffusion of the material during deposition occurs at this zone and make the bonding of adjacent filaments (between 162 and 198°C).

According to the obtained results, it was understood that the T_g is about 61°C. The reference sample shows the melting and the T_c of about 198°C and 162°C, respectively. The greatest temperature range for the filament dropping the nozzle is between the melting and the T_c. Moreover, the degree of crystallinity is about 20.51%.

3.2 | Characterization of the printed sample

A reference sample with specific process parameters was printed ($T_{liquefier}$: 240°C, print speed: 15 mm/s, layer height: 0.1 mm, platform temperature: 25°C). Then the effect of the selected process parameters (Table 1) have been taken into account to be compared with the stated reference process parameters. In this regard, physico-chemical and mechanical characterizations were

TABLE 2 The obtained values related to different properties from DMA and DSC tests

Conditions	T_g (°C)	T_c (°C)	T_m (°C)	%crystallinity
Reference	61	162	198	20.51

Abbreviation: DSC, differential scanning calorimetry.

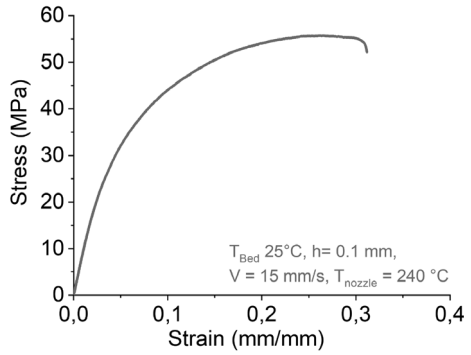

FIGURE 7 Tensile results for reference sample

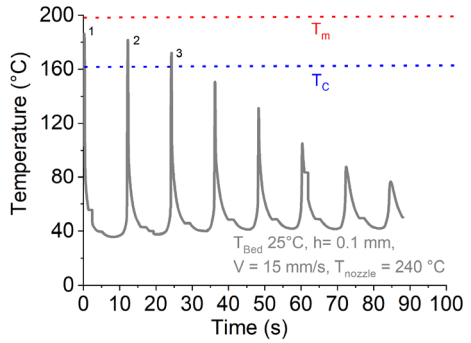

FIGURE 8 The obtained curve related to the temperature profile of the first printed layer during the deposition of other layers in the reference sample

conducted; also, the temperature profile of the first deposited layer was monitored in situ through deposition of the next deposited layers. Finally, the obtained results were utilized to evaluate the impact of each process parameter on the manufactured objects.

The obtained tensile test curve and the tensile properties values of the reference sample from the tensile test are presented in Figure 7 and Table A1 and the prepared table in the appendix section. Three samples have been tested. The failure stress and failure strain are about 60 MPa and 30%.

Some efforts were made using local measurements to record the temperature profile of the deposited consecutive layers in different locations. The recorded temperature profile was considered for the first deposited layer during the deposition of other layers in a sequence of deposition at a determined location from the commencement of deposition (Figure 8). The objective was to find out the temperature profile of the deposited consecutive layers during the FFF process by means of spot in situ measurement.

3.3 | Effect of process parameters

3.3.1 | Influence of $T_{liquefier}$

According to the conducted study, the FFF process parameters impact the temperature–time curves, which are representative of the cooling rate pattern of the printed layers.[38] The effect of the $T_{liquefier}$ as one of the most important process parameters has been considered. According to be able study the effect of $T_{liquefier}$, three different values of 220, 230, and 240°C were considered for comparing their results, according to Table 3. According to the obtained DSC curves corresponding to the printed specimens under different $T_{liquefier}$ (220, 230, and 240°C), by changing the $T_{liquefier}$ the crystallization degree and the related heat flow values of the crystallinity is changed (Figure 9, Table 3), a bit. Specifically, the related T_c value in the case of 240°C has been increased.

The obtained results from DSC curves related to the crystallinity zone were taken into account significantly. Because the diffusion and consequently the adhesion and bonding of the printed layers occurs in this zone, also it can also directly affect the dimension accuracy of the printed samples.

Figure 10 illustrates the tensile behaviors of the printed specimens under the considered and stated $T_{liquefier}$ values. The maximum tensile strength of the printed specimens under the $T_{liquefier}$ of 220, 230, and 240°C were 49 ± 1.5, 51 ± 3, and 55 ± 0.6 MPa, respectively. Also the crystallinity percentage of the manufactured samples under 220, 230, and 240°C were 19.97%, 20.26%, and 20.51%, respectively. So as it was revealed from the obtained results, by increase of the $T_{liquefier}$, the crystallinity percentage was increased, slightly. Also this (slight) increasing trend was observed in the obtained tensile strength by increase of the $T_{liquefier}$ in parallel with crystallinity increasing, in the FFF process of the CF-PA6 composite. Also the increasing evolution of Young's modulus was observed by increase of the

TABLE 3 The obtained values related to different properties from DSC curves of the printed Samples at different liquefier temperature

Conditions		T_c (°C)	T_m (°C)	%crystallinity
No. 1	$T_{liquefier} = 220°C$	161.5°C	197.5°C	19.97%
	$T_{liquefier} = 230°C$	161.7°C	197.7°C	20.26%
	$T_{liquefier} = 240°C$	162.8°C	198.7°C	20.51%

Abbreviation: DSC, differential scanning calorimetry.

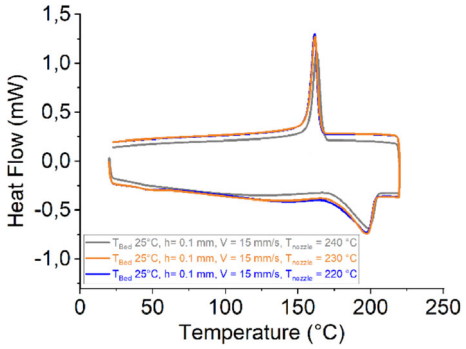

FIGURE 9 Differential scanning calorimetry (DSC**)** results for fabricated samples under the different liquefier temperatures

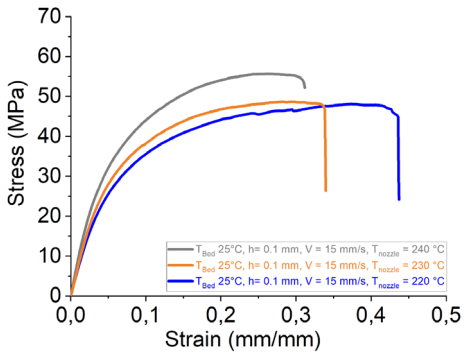

FIGURE 10 Tensile behavior of printed specimens under the various liquefier temperatures

$T_{liquefier}$ of FFF manufacturing of CF-PA6. Also according to Tian et al.,[20] in which the effect of $T_{liquefier}$ on the continuous CF reinforced PLA composites manufacturing process in the range of 180–240°C was studied. The obtained melting flow index values of PLA at the temperature of 180°C and 240°C were 2 g/10 min and 36 g/10 min, respectively. As for the obtained results, the flexural strength and modulus were increased as the temperature was increased.

Scanning electron microscopy (SEM) observations related to the $T_{liquefier}$ values of $T_{liq} = 240°C$ and $T_{liq} = 220°C$ were done and presented in Figure 11.

The existence of the micro voids between the printed layers, which caused the poor mechanical properties of the FFF manufactured specimens in comparison with the manufactured parts by conventional manufacturing methods are marked on the SEM photographs. The micro vids in the interface of the printed layers can originate from lower viscosity of PA-6 and caused the poor adhesion and poor strength of the interface of the layers, which could be the local crack propagation location and subsequence fracture. In the captured SEM photographs, the micro voids were more sensible in the related micrograph to the printed specimen at the $T_{liquefier}$ value of 220°C (less $T_{liquefier}$).

3.3.2 | Influence of print speed

The Influence of the print speed as one of the other process variables was studied. The importance of this parameter can be highlighted in terms of the production speed. For study the influence of the print speed, three different print speeds of 13, 15, and 17 mm/s were considered to print the required specimens. According to the obtained DSC curves of the printed specimens from the used different print speed (13, 15, and 17 mm/s); there is no noticeable change in the obtained degree of crystallinity values (Figure 12, Table 4).

According to the applied tensile tests on the printed specimens at the stated different print speed values, the tensile strength values of 65 ± 0.5, 55 ± 0.6, and 63 ± 1.3 were obtained related to the printed specimens at the print speed of 13, 15, and 17 mm/s, respectively (Figure 13). Also the same evolution of Young's modulus (such as the tensile strength) was observed from the obtained tensile test results related to the prepared specimens at the stated print speed values. So the tensile properties of the printed specimens at the print speed values of 13 and 17 mm/s were closer to each other in comparison with the obtained results related to manufactured samples at 15 mm/s. One can note that the degree of crystallinity of the printed sample with the print speed of 13 mm/s was slightly higher, which showed higher tensile strength, too. However, according to the SEM micrographs of the manufactured specimens at the print speed value of 13 mm/s, the micro voids at the interface of the printed layers were observed (Figure 14) and the printed sample has not good dimensional accuracy. Due

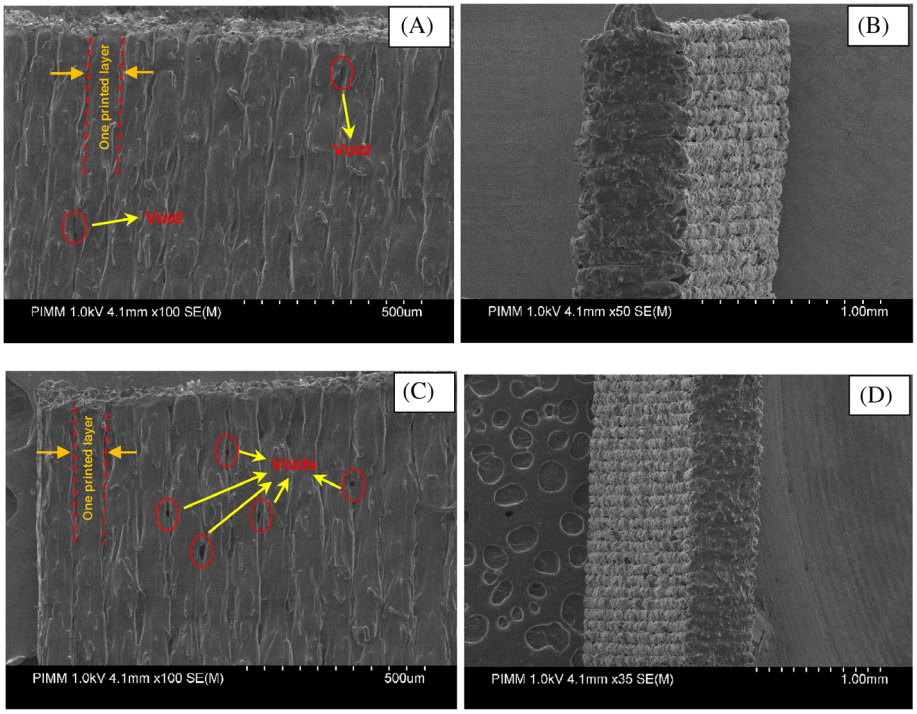

FIGURE 11 Scanning electron micrographs (SEM) related to the printed specimens at $T_{liq} = 240^{\circ}C$ (A, B) and $T_{liq} = 220^{\circ}C$ (C, D)

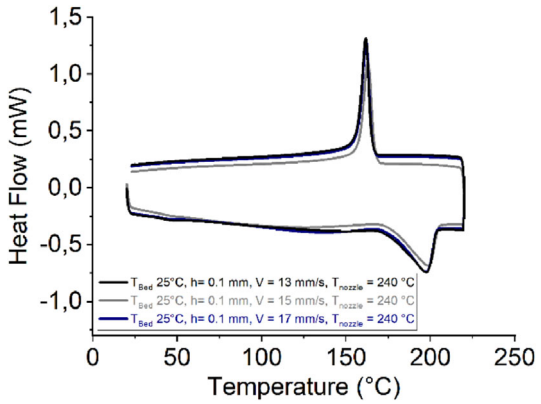

FIGURE 12 Obtained differential scanning calorimetry (DSC) curves from printed samples at different print speed

to the weak dimensional stability, it seems the printed sample with the print speed of 15 mm/s has the optimized process condition.

To analyze this phenomenon, in situ temperature measurements for different print speeds of 13, 15, 17 mm/s are presented in Figure 15. The results exhibit that by an increase of the printing speed, the temperature evolution of the first printed layer remains above the T_c in the printed specimens with the three considered printing speed values. One can note that the print speed enhancement modifies the rearrangement of polymer chains and the consequently obtained degree of crystallinity by decreasing the cooling time. The latter can be the reason for the poor dimensional stability.

3.3.3 | Influence of layer height

The effect of the layer height as one of the process parameters was studied in the FFF process of CF-PA6. Printing process was set on three different values of 0.1, 0.2, and 0.3 mm as three different layers height values for studying the impact of this process parameter on the mechanical behavior of the obtained specimens. According to the obtained tensile test results, the printed specimens with the selected layer height values of 0.1, 0.2, and 0.3 mm have tensile strength of 55 ± 0.6, 49 ± 2.5, and 56 ± 2.5 MPa, respectively (Figure 16). Also the crystallinity percentage values of 20.51, 19.27, and 21.22 were obtained related to the printed specimens with the layer height of 0.1, 0.2, and 0.3 mm, respectively (Table 5).

According to the stated results, it is proposing that there are two competitive factors in terms of the mechanical behavior of the manufactured samples by the FFF process of CF-PA6 with the different layer height (the stated layer height values). The two factors which compete with each other by increase of the layer height were (i) decrease of the liquidity (or fluidity) of the printed layers and (ii) increase of retained temperature in the printed layers. The effect of the decrease of the liquidity (or fluidity) has overcome the second competitive factor in the obtained samples by changing the layer height from 0.1 to 0.2 mm in the FFF process of CF-PA6. Which caused the decrease of the adhesion and bonding of the printed layer and consequent tensile strength of the printed samples with the layer height of 0.2 mm in

comparison with printed ones related to the layer height of 0.1 mm. The stated increase of the fluidity has been concluded from the observed peaks obtained from the temperature evolution (time–temperature) curves, in which the recorded maximum temperature value of each printed layer with layer height of 0.1 mm was more as comparing with the deposited layer with the height of 0.2 mm (Figure 17).

Also the crystallinity percentage was decreased a bit by the increase of the layer height from 0.1 to 0.2 mm. While it is proposed that the effect of the increased retained temperature in the printed layers has overcome the first competitive factor, in the case of the FFF process of CF-PA6 with the layer height 0.3 mm. According to the time–temperature curve (the bottom of the curves) related to the printed layer height of 0.3 mm (Figure 17) one can be observed that more temperature value, which can cause the polymer chains rearrangement and the consequent increase of the mechanical behavior, due to the crystallinity percentage increment.

From these results, it seems that the printed composite specimens with layer height of 0.1 mm (as reference sample) could be the optimal process parameter. Also according to Durga et al,[35] in the case of reinforced PLA by CF, it is stated the highest tensile strength observed in the sample with the minimum layer thickness (0.1 mm).

TABLE 4 The obtained values related to different properties from DSC curves of the printed samples at the different print speeds

Conditions		T_c (°C)	T_m (°C)	%crystallinity
No. 2	V = 13 mm/s	161.68°C	197.71°C	20.77%
	V = 15 mm/s	162.82°C	198.72°C	20.51%
	V = 17 mm/s	161.94°C	197.60°C	20.64%

Abbreviation: DSC, differential scanning calorimetry.

3.3.4 | Influence of bed temperature

The effect of bed temperature was analyzed at different temperature values 25, 45, 60, and 80°C. One can note that PA-6 has relatively low viscosity and by increasing the bed temperature, the risk of lack of dimensional stability can occur. Figure 18 presents the SEM micrographs related to the printed specimen at bed temperature of 80°C. One can observe that the layers were more deformed compared to the SEM micrographs of the printed sample at bed temperature of 25°C (Figure 11). Moreover, there are more voids in this case.

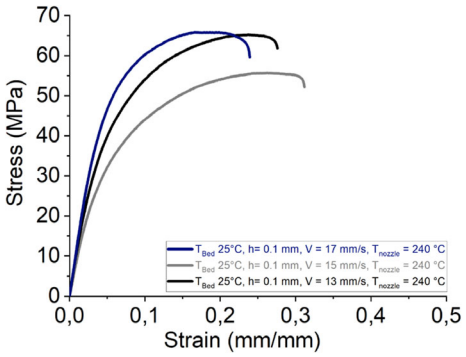

FIGURE 13 Tensile behavior of printed specimens at the different print speed values

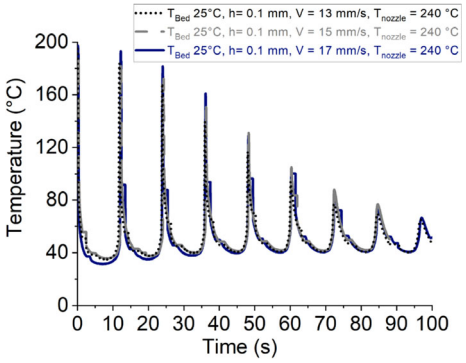

FIGURE 15 In situ temperature measurement for different print speed

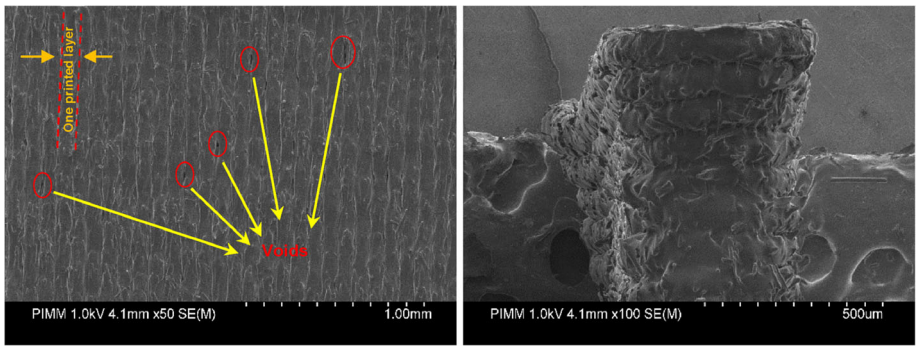

FIGURE 14 Scanning electron micrographs (SEM) related to the printed specimens at V = 13 mm/s

TABLE 5 Obtained different properties from DSC curves with the various layer height

Conditions		T_c (°C)	T_m (°C)	%crystallinity
No. 3	h = 0.1 mm	162.82°C	198.72°C	20.51%
	h = 0.2 mm	161.50°C	197.79°C	19.27%
	h = 0.3 mm	161.68°C	197.48°C	21.22%

Abbreviation: DSC, differential scanning calorimetry.

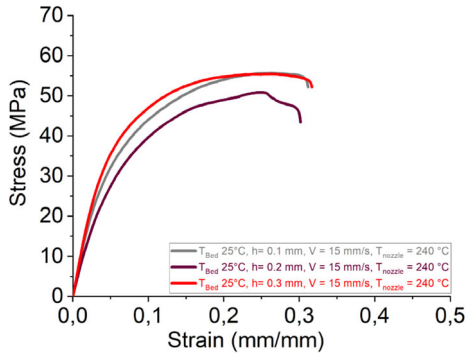

FIGURE 16 Tensile behavior of the printed specimens with the various layer height

However, according to Young-hyu choi et al.,[36] the Influence of bed temperature on heat shrinkage shape error of ABS was studied under bed temperature values of 50, 70, 90, and 110°C. It is stated that the sample with lower bed temperature has the highest deformed shape error. On the other hand, laminating adhesion became poor if the bed temperature is more than 120°C. As for explanation, the softening temperature of the used ABS polymer was reported 104°C. The interlayer adhesion of the printed layers was increased until the bed temperature value of 110°C, which was close to ABS softening temperature. This low difference between the bed temperature and ABS softening temperature caused slow phase transformation from the liquid state to solid state, which prepared slow hardening. While the bed temperature of 120°C had more difference from the ABS softening temperature, which caused poor laminating adhesion.

Figure 19 presents the in situ temperature measurement of the printed specimens with the various bed temperatures. For all printed specimens with the aforementioned different bed temperatures, after the first layer deposition, the temperature reaches lower than T_c. However, at bed temperature of 80°C, this value was near to the T_c compared to other bed

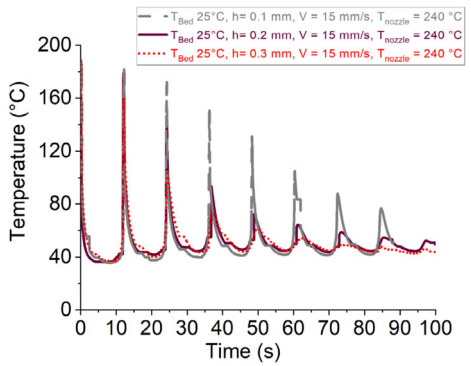

FIGURE 17 In situ temperature measurement of the printed specimens with the various layer heights

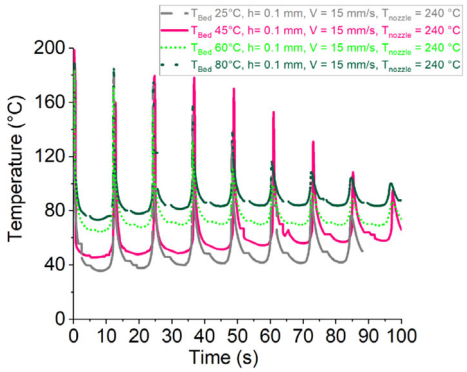

FIGURE 19 In situ temperature measurement of the printed specimens with the various bed temperatures

FIGURE 18 Scanning electron micrographs (SEM) related to the printed specimen at bed temperature of 80°C

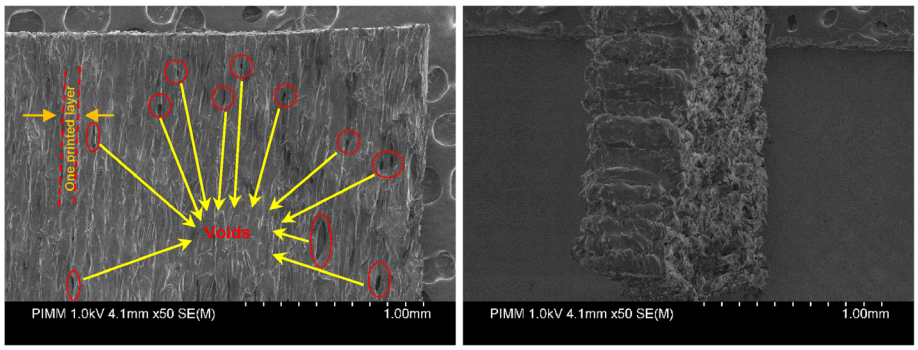

temperatures, but the problem of dimensional stability existed.

Also according to Rudolph et al.,[39] the existence and the related size of the voids influence the re-heating or cooling rate among the deposition process.

3.4 | Microstructure analysis related to the printed specimens

Figure 20 presents the microstructure observations of the manufactured specimens (10-deposited filaments) for reference condition. The aim was to understand the contact surface of two adjacent layers. Results reveal that by increase of distance from the first deposited layer, the contact surface of the adjacent layers decreased. Because of the stated temperature evolution of the deposited layers, it is observable that after two or three sequences of deposition, the temperature dropped below the T_c. This fact contributes to the rate of cooling, solidify material, less material diffusion, and then decrease the contact surface between two adjacent deposited layers.

In comparison with the reference sample, each condition prepared its effect on the final feature and microstructure of the manufactured parts. According to the aforementioned observations, the same evaluation was applied on the deposit layers (Figure 21) to evaluate the contact surface of each two adjacent filaments to be able to compare against each other. This analysis is beneficial to summarize the impact of each process parameter on the bonding and quality of manufactured parts. One can note that the reference sample has a more stable contact surface at first 10 printed layers. This analysis confirms that the reference sample (with printing condition of: $T_{liquefier}$: 240°C, print speed: 15 mm/s, layer height: 0.1 mm, and platform temperature: 25°C) produced by the best and optimal process parameter.

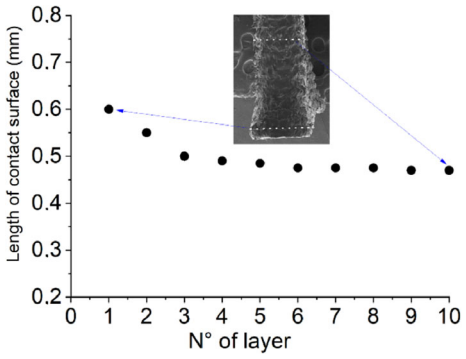

FIGURE 20 Analysis of the length of contact between two adjacent filaments (the reference sample)

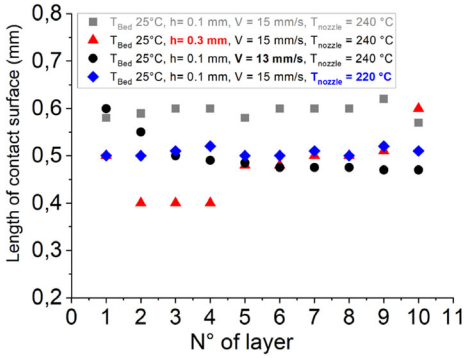

FIGURE 21 Comparing the contact length between two adjacent layer in each condition of printing

4 | CONCLUSIONS AND OUTLOOK

This paper provides an experimental investigation for the impact of some important FFF process parameters of polymer-based composites on the interlayer adhesion (bonding) of the deposited filaments. The thermal, physicochemical, and mechanical analysis showed that degree of crystallinity can affect the diffusion of the material during the cooling stage and the bonding of two adjacent filaments and consequently the mechanical properties of the final part. Temperature profile evaluation of printed layers illustrates that FFF process parameters have a significant effect on the cooling process of filaments, which modifies the bonding of adjacent filaments. Failure stress/strain can be the indicators to figure out the mechanical properties of FFF manufactured products. One can note that the polymer used in this study was PA-6, which has low molecular weight and low viscosity. To analyze the effect of process parameters in this type of materials, it is important to pay close attention to the temperature. By increasing the bed temperature, the problems of dimensional stability and voids presence can occur. The results of this paper confirm that the reference sample (with printing condition of: $T_{liquefier}$: 240°C, print speed: 15 mm/s, layer height: 0.1 mm, platform temperature: 25°C) produced the best and optimal process parameter.

ORCID

Mohammad Ahmadifar https://orcid.org/0000-0002-1783-5667

Mohammadali Shirinbayan https://orcid.org/0000-0002-2757-8529

REFERENCES

[1] A. Standard, *ASTM Int.* **2012**, F2792.

[2] M. Alimardani et al., *J. Laser Appl.* **2007**, *19*(1), 14.

[3] S. L. Ford, *J. Int. Com. Econ.* **2014**, *6*, 40.

[4] R. Hague et al., *Proc. Ins. Mech. Eng. Part C: J. Mech. Eng. Sci.* **2003**, *217*(1), 25.
[5] T. D. Ngo, A. Kashani, G. Imbalzano, K. T. Nguyen, D. Hui, *Compos. B: Eng.* **2018**, *143*, 172.
[6] R. Suntornnond, J. An, C. K. Chua, *Macromol. Mater. Eng.* **2017**, *302*(1), 1600266.
[7] D. Küpper, W. Heising, G. Corman, M. Wolfgang, C. Knizek, V. Lukic, *Get Ready for Industrialized Additive Manufacturing*, DigitalBCG, Boston Consulting Group, **2017**.
[8] F. Ning et al., *Compos. B: Eng.* **2015**, *80*, 369.
[9] W. Zeng et al., *J. Thermoplast. Compos. Mater.* **2013**, *26*(1), 125.
[10] K. Bryll, E. Piesowicz, P. Szymański, W. Ślączka, M. Pijanowski, *MATEC Web Conf.* **2018**, *237*, 2006.
[11] F. Bárnik, M. Vaško, M. Sága, M. Handrik, A. Sapietová, *MATEC Web Conf.* **2019**, *254*, 1018.
[12] Y. Zheng, Y. Wang, R. K. Chen, S. Deshpande, N. S. Nelson, S. R. Buchman, A. J. Shih, *Rapid Prototyp. J.* **2017**.
[13] J. Butler, *Assem. Autom.*, *31*(3), 212.
[14] J. P. Kruth, L. Froyen, V. J. Van, et al., *J. Mater. Process Technol.* **2011**, *149*(1–3), 616.
[15] A. C. Taylor, S. Beirne, G. Alici, G. G. Wallace, *Rapid Prototyp. J.* **2017**.
[16] F. Ning, W. Cong, Y. Hu, H. Wang, *J. Compos. Mater.* **2017**, *51*(4), 451.
[17] K. V. Wong, A. Hernandez, *ISRN Mech. Eng.* **2012**, *1*, 1.
[18] N. Li, Y. Li, S. Liu, *J. Mater. Process. Technol.* **2016**, *238*, 218.
[19] Y. Chuncheng, *Rapid Prototyp. J.* **2017**, *23*(1), 209.
[20] X. Tian, T. Liu, C. Yang, Q. Wang, D. Li, *Compos. Part A: Appl. Sci. Manuf.* **2016**, *88*, 198.
[21] K. I. Mori, T. Maeno, Y. Nakagawa, *Proc. Eng.* **2014**, *81*, 1595.
[22] Y. Nakagawa, K. I. Mori, T. Maeno, *Int. J. Adv. Manuf. Syst.* **2017**, *91*(5–8), 2811.
[23] M. Namiki, M. Ueda, A. Todoroki, Y. Hirano, R. Matsuzaki, *Soc. Adv. Mater. Process Eng.* **2014**, January.
[24] A. Camposeo, L. Persano, M. Farsari, D. Pisignano, *Adv. Optic. Mater.* **2019**, *7*(1), 1800419.
[25] X. Wang, M. Jiang, Z. Zhou, J. Gou, D. Hui, *Compos. B: Eng.* **2017**, *110*, 442.
[26] F. W. Liou, *Rapid Prototyping and Engineering Applications: A Toolbox for Prototype Development*, Crc Press, **2007**.
[27] D. S. Ertay, A. Yuen, Y. Altintas, *Addit. Manuf.* **2018**, *19*, 205.
[28] D. Stoof, K. Pickering, *Compos. B: Eng.* **2018**, *135*, 110.
[29] F. C. Campbell Jr.., *Manufacturing Processes for Advanced Composites*, Elsevier, **2003**.
[30] H. Prüß, T. Vietor, *J. Mech. Des.* **2015**, *137*(11).
[31] A. Chadha, M. I. U. Haq, A. Raina, R. R. Singh, N. B. Penumarti, M. S. Bishnoi, *World J. Eng* **2019**.
[32] S. R. Rajpurohit, H. K. Dave, *Rapid Prototyp. J.* **2018**.
[33] G. Ćwikła, C. Grabowik, K. Kalinowski, I. Paprocka, P. Ociepka, *IOP Conf. Ser. Mater. Sci. Eng.* **2017**, *227*(1).
[34] K. J. Christiyan, U. Chandrasekhar, K. Venkateswarlu, *IOP Conf. Series Mater. Sci. Eng.* **2016**, *114*, 12109.
[35] V. D. P. Rao, P. Rajiv, V. N. Geethika, *Mater. Today Proc.* **2019**, *18*, 2012.
[36] Y. H. Choi, C. M. Kim, H. S. Jeong, J. H. Youn, *WJET* **2016**, *4*(3), 186.
[37] M. Ramesh, K. Panneerselvam, *Mater. Today Proc.* **2020**.
[38] A. Kallel, E. Babaeitorkamani, I. Koutiri, A. Khavandi, M. Tamizifar, M. Shirinbayan, A. Tcharkhtchi, *Int. Polym. Process. J. Polym. Process. Soc.* **2019**, *34*(4), 434.
[39] N. Rudolph, J. Chen, T. Dick, *AIP Conf. Proc.* **2019**, *2055*(1), 140003.

How to cite this article: K. Benfriha, M. Ahmadifar, M. Shirinbayan, A. Tcharkhtchi, *Polym. Compos.* **2021**, 1. https://doi.org/10.1002/pc.26282

APPENDIX A.

TABLE A1 Tensile results for the reference sample

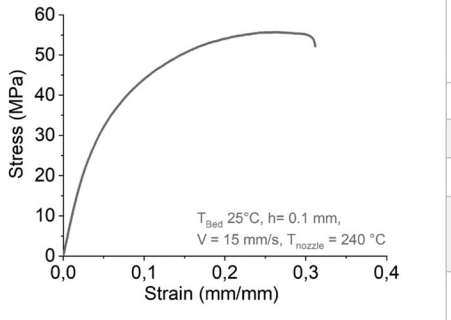

Sample	E (MPa)	σ_{max} (MPa)	ε_{max}	σ_y (MPa)	ε_y
1	950	55.7	0.26	13.6	0.02
2	850	54.9	0.28	15.7	0.02
3	1000	54.5	0.22	17.8	0.02
Average	950	55	0.25	15.7	0.02
STDEV	100	0.6	0.03	23.7	0

Tensile results for the reference sample